Neutral air turbulence in the mesosphere and associated polar mesospheric summer echoes (PMSEs)

Alireza Mahmoudian[1], Mike J. Kosch[2,3,4], Wayne A. Scales[5], Michael T. Rietveld[6], and Henry Pinedo[7]

[1]Institute of Geophysics, University of Tehran, Iran.
[2]Department of Physics, Lancaster University, Lancaster, UK.
[3]South African National Space Agency (SANSA), Hermanus, South Africa
[4]Dept. of Physics and Astronomy, University of the Western Cape, Bellville, South Africa
[5]Bradley Department of Electrical and Computer Engineering, Virginia Tech.
[6]EISCAT Scientific Association, Ramfjordmoen, Norway
[7]Department of Physics and Technology, University of Tromsø, Tromsø, Norway

Correspondence: Alireza Mahmoudian (a.mahmoudian@ut.ac.ir)

Abstract.

The first true common volume observations of the PMSE source region with 4 radars are presented in this paper. Radar frequencies of 8, 56, 224, and 930 MHz are used in this study. Three days of experimental observations at EISCAT are presented. Numerical simulations of mesospheric dusty/ice plasma associated with the observed radar frequencies are presented. The effect of neutral air turbulence on the generation and strength of plasma density perturbations associated with PMSE using four radar frequencies and in the presence of various dust parameters is investigated. Using the model it is shown that the well-known neutral air turbulence in the presence of heavy dust particles and neutral air turbulence combined with dust density (dusty turbulence) can largely explain the observed radar cross-section at four radar frequencies. The effect of neutral air turbulence amplitude along with dust charging and diffusion in the presence of various dust parameters is investigated using the computational model. Specifically, the response of diffusion to charging time scales, plasma density fluctuation amplitude and background dusty plasma parameters are discussed. Several key parameters in the dusty plasma responsible for the PMSE observations are determined. Qualitative comparison of radar echo strength at 4 frequencies with numerical results is provided. Unlike the previous studies that required large dust particles of 20 nm for PMSE formation, the present work demonstrates the possibility of small dust particles to explain the experimental observations.

1 Introduction

So-called Polar Mesospheric Summer Echoes PMSEs are very strong coherent radar echoes produced by electron density fluctuations at half the radar wavelength (Bragg scatter condition) in the summer polar mesosphere (80-90 km). While polar mesospheric echoes have been observed in the absence of neutral air turbulence in some cases (Lubken et al., 1993; 2002),

20   theoretical studies by Hill et al. (1999) and Rapp and Lubken (2004) have shown that coupling of the neutral air turbulence with the dusty plasma is the main driving source for PMSE and the associated electron density fluctuations in the mesopause region. Without including dust particles of meteoric origin, the small-scale electron density fluctuations produced through coupling of neutral air turbulence with electron density fluctuations diffuse out very quickly due to the high viscosity effect. The Schmidt number Sc is defined as a ratio of viscosity ν to electron diffusion coefficient D ($Sc = \nu/D$) (Lubken et al., 1998). It is unity

25   if dust particles are excluded. The spectrum of velocity fluctuations in a turbulent medium scales as $k^{-5/3}$ where k is the wavenumber. It has been shown that the presence of aerosol particles in the mesosphere can increase the Schmidt number to values much greater than unity and extend the viscous cut-off (Cho et al., 1992; Cho and Kelley, 1993; Cho and Rottger, 1997). In addition to the role of charged aerosols in reducing the diffusion timescale of electron density fluctuation, charged aerosols may also result in radar scatter. The so-called dressed aerosol scatter may increase radar scatter above the incoherent scatter

30   and is not dependent on radar wavelength. This theory can explain the observed PMSE using UHF radars. Electron density fluctuations observed in recent in-situ measurements using rocket probes have shown a good agreement with the theory of neutral air turbulence coupling with charged species (Rapp and Lubken, 2004; Lie-Svendsen et al., 2003). The present study is the first attempt to provide a detailed study on dusty plasma parameterization of radar echoes in the presence of mesospheric neutral air turbulence and dust particles.

35   The computational modeling of mesospheric plasma mixed with ice/dust particles which are capable of attracting free ions and electrons has been studied by Lie-Svenson et al. (2003) and Scales (2004). These first studies developed the concept of charging of the mesospheric electrons onto irregular dust density leave electron density "fingerprints" in the form of the electron irregularities that produce PMSE. More simulation work has been done to investigate the temporal evolution of electron irregularities in response to radio wave heating (Chen and Scales, 2005; Mahmoudian et al., 2011; Senior et al., 2014; Mah-

40   moudian et al., 2017a). Very recent work by Mahmoudian et al. (2018) is dedicated to the time evolution of PMSE during enhanced electron density in the mesosphere produced by electron precipitation events. This work demonstrated that the ratio of electron density fluctuation amplitude (δn_e) to the plasma density (n_e) plays a critical role in the appearance/disappearance of the layer. The simulation results also revealed that the existence of PMSE is mainly determined by dust radius and dust density.

45   The coupling of the neutral air turbulence with mesospheric dusty plasma as a generation source of fluctuations in plasma and dust densities as well as electric field was investigated by Mahmoudian et al. (2017b). The impact of the neutral air turbulence wavelength spectrum in the presence of charged dust particles was studied and the extension of the smaller wavelength electron density fluctuation diffusion timescales ~~in smaller wavelength~~ was considered. The coupling of neutral air turbulence with mesospheric dusty plasma including the steady state balance for charging and diffusion on the plasma density fluctuations was

50   investigated by Mahmoudian et al. (2017b). Therefore, the present study provides the first multi-frequency observations of PMSE from 8 MHz up to 930 MHz (corresponding to electron density fluctuation wavelength ~ 40 m to 16 cm, respectively) as well as the time evolution of plasma density fluctuations in numerical modeling of dusty plasma irregularities within the associated radar wavelengths. The diffusion and charging processes, electron and ion density variation, and electron density fluctuation amplitude corresponding to the radar echoes are studied for a variety of background dusty plasma parameters. While

55 theoretical models fall short in predicting the dusty plasma parameters associated with the observed PMSEs, numerical results used in this paper to determine the background parameters as well as provide an explanation for the non-existence (strong weakening) of PMSE at 930 MHz. The agreement between the numerical simulations and four radar frequency observations of the PMSE source region simultaneously are presented and discussed.

2   Experimental observations

60 The data collected during 2012 and 2013 research campaigns at the EISCAT HF Facility at Ramfjordmoen, Norway (69.6°N, 19.2°E), are presented in this paper. The HF radar at ~ 8 MHz (7.9 MHz) was built using the divided HF heater array as the HF radar transmitter. While 10 transmitters on Array 1 where used for heating the ionosphere by radiating vertically in O-mode polarization at 6.77 MHz (an effective radiated power (ERP) of about 600 MW), simultaneously, the Facility operated in radar mode radiating vertically using two transmitters at 7.953 MHz on Array 1. The pump was cycled 48 s on and 168 s off starting

65 at 09:00 UT for the cases of 10 June 2013 and 26 July 2013. The HF heater alternated between O- and X-mode polarization. The HF radar transmission used a pair of 20 baud complementary codes (10 μs bauds and 1.5 km range resolution). The receiving antenna O-mode gain was 25.2 dBi. The O-mode-transmitted pulses received using O-mode polarization separation are used in this study. A complete measurement cycle took 80 ms. It should be noted that the HF radar data presented in this paper are not calibrated for the D-region absorption. The HF radar RCS (radar cross-section) is used in this paper to denote

70 that the effect of ionospheric absorption is not taken into account. Echoes were received digitally and combined in software to produce O or X polarization using Array 3 from two orthogonal linear polarizations. The ~~Morro~~ (the MObile Rocket and Radar Observatory) radar at 56 MHz was used to measure the PMSE on the border line of the HF and VHF bands (Havnes et al., 2015). The ~~Morro~~ radar was established at EISCAT in 2008 and decommissioned in 2016 (Pinedo et al., 2014). The EISCAT 224 MHz and 930 MHz radars monitored the mesospheric echoes in the same direction (Næsheim et al., 2008). The

75 VHF radars (56 MHz and 224 MHz) are not significantly affected by absorption.

Figure 1 shows the simultaneous PMSE observations with 4 radar frequencies. The UHF (930 MHz) radar observation is shown in the top panel and was stopped due to a technical issue around 11:30 UT. The background electron density of order 10^{11} m^{-3} extends to 80 km altitude where the PMSE associated dust/ice particles form. The VHF radar (224 MHz), shown in the second panel from top, also represents the background electron density with a similar magnitude as those observed

80 with the UHF radar. The VHF radar also shows simultaneous coherent PMSE that corresponds to electron density fluctuation wavelength of ~ 67 cm. The third panel shows the radar backscatter from the polar mesospheric clouds at 56 MHz. The lower panel shows the HF PMSE at 8 MHz which is obtained using the Software Defined Radio Receiver (SDR) radar in conjunction with the EISCAT HF facility. As observed in Figure 1, no PMSE is depicted at UHF (corresponding electron density fluctuation wavelength of 16.5 cm) during the time of operation. The VHF echoes appear between ~ 80-87 km starting around 10:30 UT.

85 The VHF PMSE extends to altitudes lower than 85 km and becomes much stronger after 12:00 UT. While the overall shape of the PMSE layer looks very similar at 56 and 224 MHz, a clear extension and presence of the PMSE layer even before 10:30 UT can be seen in the Morro radar observations. The HF radar ~~has~~ received backscattered echoes from the beginning of the

observations at 8:00 UT. The HF echoes show a much stronger pattern and extended over a wider altitude range in comparison with the 56 and 224 MHz echoes. Therefore the observations show consistency with the well developed theory of neutral air turbulence which predicts an extension of turbulence to higher wavenumbers (k) (smaller irregularity wavelength λ) by including the reduced diffusion of fluctuations in the presence of heavy dust particles. This is mainly considered as the source of dusty plasma fluctuations and associated radar echoes (PMSE). Therefore, this will be subsequently investigated quantitively using numerical simulations. The HF echoes appear at a higher altitude range between 85 km to 90 km (8:00 UT-11:00 UT). A slow descent in altitude to the ranges around 85 km is seen for times after 11:30 UT which is in agreement with the observed 56 and 224 MHz echoes. As discussed in the introduction, the theoretical models are still incapable of characterizing the observed radar echoes in terms of strength and duration with realistic dusty plasma parameters corresponding to the PMSE source region.

Figure 2 shows a similar experimental set up to Figure 1 (excluding 930 MHz radar observations due to technical issues). A stable PMSE layer can be seen from the beginning of the observations at around 09:00 UT on 19 June 2013 at 56 MHz and 224 MHz. The overall shape of the layers including the layering phenomenon between 9:50 UT and 11:20 UT as well as the curving structure around 12:30 UT can be clearly seen at both 56 and 224 MHz. The comparison between the two frequencies illustrates that the VHF echoes reach a very large amplitude at some times during the experiment and over a narrow altitude range (10:00 -11:00 UT). The heating modulation effects including the suppression of radar echoes after the HF heater turn-on and slow recovery to the background unperturbed echoes after the turn-off overshoot effect can be seen in the 56 and 224 MHz echoes (Havnes et al., 2015). Although the signature of HF pump modulation can be seen in the data, the overall intensity of the echoes at both frequencies remains intact. La Hoz et al. (2006) have also shown that a large increase in the electron temperature does not affect mesospheric neutral turbulent state as an external driver for PMSE. This will make it possible to use the data presented here as a benchmark for comparison with the numerical simulations presented in the following section in order to investigate neutral air turbulence effects on the formation of plasma irregularities. The overall range of presence in altitude and intensity of 56 MHz echoes is higher in comparison with the 224 MHz echoes. The HF echoes are much stronger in comparison with 56 and 224 MHz, and cover a much wider altitude range. As can be seen in Figure 2, the 8 MHz echoes start around 84 km and extend to $\sim$ 91 km. Towards the end of experiment the lower bound of HF echoes reaches $\sim$ 80 km (after 11:00 UT). No layering structure is seen in 8 MHz echoes. It's noteworthy that the HF radar data are not calibrated for the lower ionospheric absorption which appeared to be of order a dBs (Senior et al., 2014).

Figure 3 includes the PMSE at all 4 radar frequencies available at EISCAT on 26 July 2013 between 9:00 UT and 13:00 UT. The UHF (930 MHz) echoes imply the background mesospheric conditions were quiet during this experiment. The UHF data shows a weak PMSE layer around 82 km starting at 11:40 UT to 12:00 UT. All other three radars used in the experiment show the existence of PMSE at various strengths. The 224 MHz radar show discontinuous echoes centered around 84 km. While the lower VHF PMSE layers continue to 11:30 UT, a much stronger and double 224 MHz echo layer appeared between 85 to 87 km. Similar behavior of a layered structure to Figure 2 is observed at 56 and 224 MHz, although the 8 MHz radar shows a continuous layer of echoes in time between 09:00 to 11:00 UT. The overall intensity of the HF echoes is much higher than at 56 and 224 MHz. Such a difference can be seen for 224 MHz in comparison with 930 MHz. This effect will be investigated throughout this paper using numerical simulations of the perturbed mesospheric dusty plasma with different

background parameters. This study aims to further elucidate the theory of neutral air turbulence as the source of mesospheric plasma density fluctuations responsible for coherent radar echoes and in the proximity of dust particles. The size and density of

125 dust particles along with the initial amplitude of irregularities within dust density as a result of coupling with neutral turbulence will be investigated.
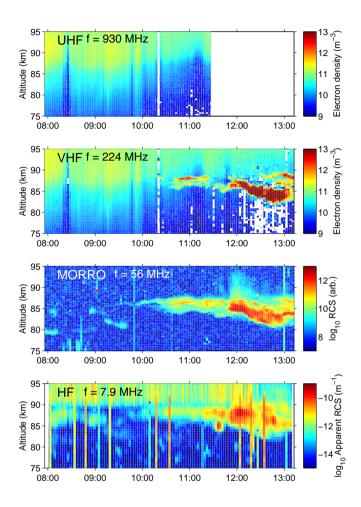

Figure 1. Simultaneous PMSE observations using 930 MHz, 224 MHz, 56 MHz, and 8 MHz radars, respectively from the top to the bottom, at EISCAT. The experiment was conducted on 12 July 2012 between 8:00 UT to 13:10 UT.
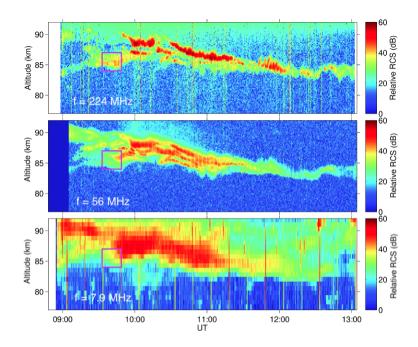
Figure 2. Simultaneous PMSE observations using 224 MHz (top), 56 MHz (middle), and 8 MHz (bottom) radars at EISCAT. The experiment was conducted on 19 June 2013 between 9:00 UT to 13:00 UT. The wavelength associated with each panel corresponding to the radar frequency is shown.

3 Numerical Model

The effect of dust particles on density fluctuations in PMSE region was first investigated using a computational model by Lie-Svendsen et al. (2003). They developed a multi-fluid model that could only consider about 6 or so dust particle sizes. Transport due to gravity, multipolar diffusion, and discrete charging model were also used (LieSvendsen et al., 2003). This model was used to explain the correlation and anti-correlation between electron and ion density fluctuations in the mesopause region. Scales (2004) developed a similar hybrid model including fluid plasma and particle in cell (PIC) dust with continuous dust charging process. The Scales (2004) model can use arbitrary size/mass/radius/charge distributions and can therefore more realistically model the mesospheric dusty plasma behavior. ~~Continuous~~ charging model based on the Orbital-Motion-Limited (OML) approach has been used for the time varying charge on the dust particles. It should be noted that the difference between the continuous charging model and discrete charging model based on statistics is negligible in this circumstance (Chen and Scales, 2005).
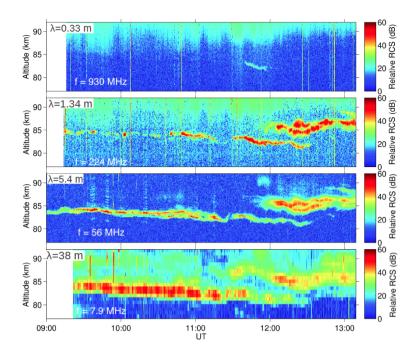
6

Figure 3. Simultaneous PMSE observations using 930 ~~MHz~~, 224 ~~MHz~~, 56 ~~MHz~~, and 8 MHz radars, respectively from the top to the bottom, at EISCAT. The experiment was conducted on 26 July 2013 between 9:00 UT to 13:00 UT.

The summer mesopause temperature for both ions and electrons is taken to be $T_e = T_i = 150$ K. The collision of charged dust with neutrals is implemented by using a Langevin method (Winske and Rosenberg, 1998) and the dust-neutral collision

140 frequency is denoted by ν_{dn}. The initially uncharged dust is taken to have density given by

$$n_d(x) = n_{d0}\left(1 + \frac{\delta n_{d0}}{n_{d0}}\sin(2\pi mxl)\right) \tag{1}$$

where n_{d0} is the undisturbed density, δn_{d0} is neutral dust irregularity amplitude, m is the mode number, and l is the system length of the model. In the current model, the plasma irregularities ultimately result from charging of the electrons onto this irregular dust density. The mechanism for the generation of the dust irregularities is discussed in Mahmoudian et al. (2017b).

145 One way of understanding the response of the electron density fluctuation amplitude to the background dust plasma parameters is to use the analytical expression for the timescale of physical processes that actually affect the density fluctuations. In general two processes (1) charging (electron/ion attachment to the dust particles) and (2) plasma density diffusion determine the steady state amplitude of fluctuations in the plasma density. The diffusion process tends to smooth out irregularities and

the diffusion timescale τ_{diff} approximated for the natural PMSE layer ($T_e/T_i = 1$) by (Chen and Scales, 2005; Mahmoudian et al., 2011):

$$\tau_{diff} \approx \nu_{in} \left(\frac{\lambda_{irreg}}{2\pi v_{thi}} \right)^2 \frac{1}{\left(1 + \left(1 + \frac{z_{d0} n_{d0}}{n_{e0}} \right) \right)} \tag{2}$$

where ν_{in}, z_{d0}, $n_{e,(d)}$ λ_{irreg} and v_{thi} are the ion-neutral collision frequency, charge density on the dust particles, electron (dust) density, electron density irregularity wavelength and ion thermal velocity, respectively. Equation (2) implies the importance of the dependence of the diffusion time on the irregularity wavelength λ_{irreg}.

The timescale for electron attachment onto the dust is approximated by (Mahmoudian et al., 2011):

$$\tau_{chg} \approx \frac{1}{\sqrt{8\pi} r_d^2 v_{te0} e^{-4.1} n_{d0}} \tag{3}$$

~~while~~ such simple theoretical expressions predict the dependency of radar echoes on the background dusty plasma parameters, they are unable to predict the steady state amplitude of irregularities under varying background dust and neutral parameters (δn_e^2) responsible for radar echoes. Therefore, the computational model is incorporated in this paper to study the characteristics of radar echoes with respect to the dusty plasma parameters. As can be seen in Eq. (1), the diffusion timescale depends on the λ_{irreg}. The numerical simulations presented in this paper are associated with radar frequencies slightly different from the observations due to a limitation of the model having a discrete spatial grid. The difference is of the order of a few centimeters in fluctuation wavelength, and are not expected to change the physical processes and the results.

The summer mesopause temperature for both ions and electrons is taken to be $T_e = T_i = 150$ K. The ion-neutral collision frequency is of order 10^5 s^{-1}. The electron density is assumed to be 2×10^9 m^{-3} (Robertson et al., 2009). The numerical simulations presented in this paper include a wide range of dusty plasma parameters such as small and large dust particles as well as various dust densities. The dust parameters used in this paper are summarized in Table 1. This is mainly to test the proposed theories such as dusty turbulence in order to explain the observed PMSE at a small wavelength where the original neutral turbulence has disappeared due to kinematic viscosity and turbulence energy dissipation. It should be noted that there are several theories proposed to justify why the electron diffusion survived long after the source (neutral air turbulence) has stopped but this is still an open question in community. La Hoz et al. (2006) used the theoretical model of Hill (1978) which included multipolar diffusion to determine the associated Schmidt numbers. The results required a large number of electrons (of the order of 10) on the dust particles for enhanced scattering beyond the Batchelor scale (Batchelor, 1959). Such a high charge number density may result in an electron density bite-out and is far from the range of dust radii observed using sounding rockets in the polar mesosphere (Robertson et al., 2009). A close comparison of computational results with the radar observations will be discussed in the following section to determine the most important dusty plasma parameters responsible for the long duration of small scale plasma density fluctuations in the PMSE region.

Table 1. Dusty plasma parameters used in the simulations associated with Figure 4-7.

dust parameters	dust radius (r_d)	dust density (n_d/n_{e0})	dust density fluctuation amplitude ($\delta n_d/n_d$)
Case 1	3 nm	90%	50% and 100%
Case 2	3 nm	150%	50% and 100%
Case 3	10 nm	10%	50% and 100%
Case 4	10 nm	**70%**	50% and 100%

4   Numerical results

The time evolution of 3 parameters in the simulations are considered in this study. These parameters include electron density fluctuation amplitude squared (δn_e^2) equivalent to radar echoes, diffusion to charging time scales (τ_{diff}/τ_{chg}), and time evolutions of the electron and ion densities, which corresponds to the electron density depletion as a result of charging on to dust particles. The model ran to reach the steady state condition assuming the formation of dust/ice particles in the vicinity of mesospheric plasma. The τ_{diff}/τ_{chg} value is a critical parameter that governs the time evolution and determines the steady state amplitude of electron density fluctuation amplitude (radar backscatter amplitude). The electron density is studied in order to investigate the electron depletion level as a parameter that also influences the backscattered radar signal as well as the ion density to monitor the quasi-neutrality condition in the dusty plasma. The electron density fluctuation amplitude starts to increase initially due to the dominant charging process. As the diffusion time scale becomes comparable to the charging timescale, it slows down the increase of the electron irregularity amplitude until they both reach a steady state. Such a condition is achieved when the dust particles are saturated by the electron/ion charging currents. According to τ_{diff}/τ_{chg}, for small dust particles of 3 nm and 10 nm this condition is satisfied within 180 sec and $\sim$ 80 sec, respectively (Figures 4-7). The initial fluctuation amplitude in the dust density ($\delta n_d/n_d$) which is caused by neutral air turbulence produces a footprint in the background density. As will be discussed shortly, an increase of $\delta n_d/n_d$ from 0.5 to 1 causes a substantial increase in δn_e^2. Therefore, this parameter has a great impact on the corresponding radar echoes in different frequency bands. The black, red, blue and green colors are used in Figures 4-7 for the radar frequencies 7.3 ~~MHz~~, 58 ~~MHz~~, 234 ~~MHz~~ and 930 MHz, respectively.

The results associated with smaller dust radius of 3 nm are shown in Figures 4 and 5. According to these figures, the ion density reaches values higher than the equilibrium condition due to the low ion charging rate with respect to electron charging and in comparison with the production rate (photoionization). For larger dust particles of 10 nm, the ion density reduces as a result of ion charging process on to the dust particles. Such a reduction is of ~~the~~ order ~~of~~ 2% and 15% for dust densities of 10% and 70% (n_d/n_{e0}), respectively. One of the main characteristics that can be seen in the electron density depletion at various wavelengths (radar frequencies) is the symmetrical behavior. The average electron density (total depletion) is independent of radar frequency. The depletion level reaches $\sim$ 20%, 35%, 12%, and 70%, in Figures 4-7, respectively. A very small discrepancy in the averaged electron density reduction is seen for large dust particles of 10 nm and a high dust density of 70% (n_d/n_{e0}) (Figure 7c). This is of order 2%, which is negligible. This behavior excludes the idea that electron density depletion could contribute directly to the PMSE. Such effects imply the coherent nature of the PMSE. Figures 4a, 5a, 6a, and 7a show the time

evolution of δn_e^2, which is a proxy for the radar echoes. The right axis in panel a denotes the corresponding radar echo in dB. The values are calculated assuming $\delta n_d / n_d = 100\%$. For the solid curves associated with $\delta n_d / n_d = 50\%$, the values should be reduced by $\sim$ -0.7 dB.

Another unique feature observed in the numerical simulations is the temporal evolution of δn_e^2. While for low densities (independent of dust radius) a slow increase in δn_e^2 amplitude to a steady state value is observed (Figures 4a and 6a), for higher dust densities an overshoot effect and then a slow decrease to the steady state value is seen (Figures 5a and 7a). Such behavior is mainly due to the high initial charging process associated with more dust particles present in the plasma. This phenomena can be clearly seen in the τ_{diff} / τ_{chg} plot for $r_d = 10$ nm, $n_d / n_{e0} = 70\%$ (Figure 7b). According to this figure, a sharp decrease in τ_{diff} / τ_{chg} for values below 10^{-6} around 40 sec shows the dominant diffusion process that results in a slow decrease in δn_e^2 amplitude.

The temporal evolution of the electron density fluctuation amplitude associated with four parameter regimes are examined in this paper. The four parameter set-ups are chosen based on the major parameters that could affect the radar echoes. According to the charging and diffusion timescales that determine the steady state value of radar echoes (electron density fluctuation amplitude at different wavelengths), dust radius r_d, dust density n_d, and dust density fluctuation amplitude δn_d are considered to vary in the simulations. We assumed the heating modulation by the EISCAT HF pump has a minimal effect on the time evolution of radar echoes over 4 hours of observations ($T_e / T_i = 1$). The δn_e^2 and the corresponding radar echoes increases significantly with increasing n_d. A comparison of the results associated with the same dust radius (for example 3 nm) shows an increase of δn_e^2 by a factor of 2 for all radar frequencies (irregularity wavelengths) as the n_d increases from 90% to150%. A general empirical relationship for an increase of δn_e^2 by a factor of $\sim (n_{d2} / n_{d1})^{(6/5)}$ is obtained based on the computational results for the same dust radius.

One of the main features that has been observed in the numerical results is that the τ_{diff} / τ_{chg} for the radar frequencies of 234 MHz and 936 MHz are on the same order. As can be seen in Figures 4-7, changing the background dusty plasma parameters may vary the δn_e^2 values which corresponds to the radar echoes, but the diffusion and charging time scales stay about the same. A small difference in the estimated amplitude of δn_e^2 for similar dust parameters associated with the 224 ~~MHz~~ and 930 MHz radars contradicts the observational data. Considering that the observed UHF echoes are expected to be ~~in~~ a similar altitude range as other radar frequencies, the background dust parameters such as r_d and n_d should be the same in the simulations. Therefore, a close comparison between the δn_e^2 for 234 ~~MHz~~ and 936 MHz from the simulations with the same r_d and n_d, reveals a very small difference in the amplitude. Such numerical prediction requires the observation of PMSE at 930 MHz. This is not consistent with the observations. The numerical estimation of δn_e^2 for reduced $\delta n_d / n_d$ values from 1 to 0.5 shows that the expected radar echoes are estimated to decrease by at least 1 dB.

5   Discussion

The previous studies have shown that the small-scale electron density fluctuations produced through coupling of neutral air turbulence and charging process of electrons onto irregular dust density may be extended to higher k values (corresponding
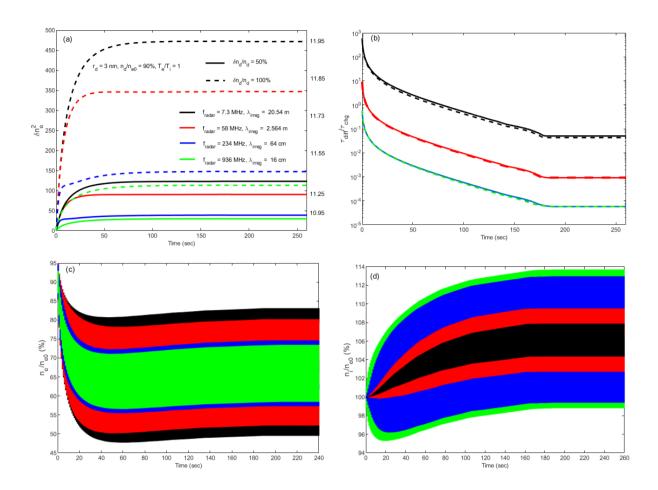
Figure 4. Numerical results associated with radar frequencies of 7.3 MHz ($\lambda_{irreg} = 40.96m$), 58 MHz ($\lambda_{irreg} = 5.12m$), 234 MHz ($\lambda_{irreg} = 1.28m$), and 936 MHz ($\lambda_{irreg} = 32cm$). The mesospheric plasma parameters are $r_d = 3$ nm, $n_d/n_{e0} = 90\%$, $T_e/T_i = 1$. The dashed lines correspond to the the initial dust fluctuation amplitude with respect to the background dust density $\delta n_{d0}/\delta n_d = 100\%$, and solid lines denote $\delta n_{d0}/\delta n_d = 50\%$. panel (a) shows the time evolution of electron density fluctuation amplitude squared (δn_e^2), which is a proxy for the radar echoes. The right axis denotes the corresponding radar echo in dB. panel (b) represents the diffusion to charging time scales associated with each radar echo. Panel (c) shows the normalized electron density variation due to charging process on to the dust particles. panel (d) shows time evolution of the normalized ion density variation to the background electron density. The colors in all panels are coded to wavelength. The mean value is used in panel (c) to determine the average electron density depletion.

to smaller wavelength). Such effect could explain the coherent PMSE echoes observed at higher radar frequencies. While the increase of the Schmidt number to values much greater than unity (in the absence of dust particles) and extension of the viscous cut-off have been shown to some extent, no clear observational and computational modeling of PMSE at various frequency bands has been introduced.
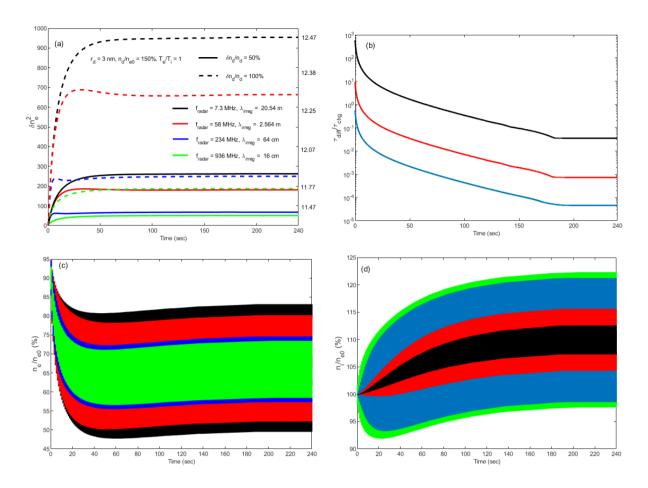
240

11

Figure 5. Similar to Figure 4 for $r_d = 3$ nm, $n_d/n_{e0} = 150\%$, and $T_e/T_i = 1$.

This paper provides the first simultaneous observations of the PMSE source region with 4 ground-based radars. The radar frequencies of 8 ~~MHz~~, 56 ~~MHz~~, 224 ~~MHz~~, and 930 MHz corresponding to Bragg scatter (coherent) electron density fluctuation wavelengths of $\lambda_{irreg} = 40.96$ m, 5.12 m, 1.28 m, and 32 cm, respectively, were employed. Such a wide range of radar frequencies cover the irregularity wavelength regimes associated with the neutral air turbulence theory. This paper investigates the time evolution and steady state amplitude of the electron density fluctuation (δn_e^2) in the presence of naturally perturbed mesospheric dust layers. The numerical calculation of δn_e^2 could be compared quantitively with the experimental observations of coherent radar echoes in various frequency bands. Since the initial modulation of the dust density profile by the background neutral density profile has a great impact on the corresponding electron density fluctuation amplitude and radar echoes, two values of 0.5 and 1 are assumed for the $\delta n_d/n_d$ parameter. Then plasma processes including electron/ion attachments to the background dust particles as well as electron density diffusion are allowed to develop and reach a steady state condition. Several background dusty plasma parameters including dust density and ~~dust~~ radius are varied in order to determine the corresponding
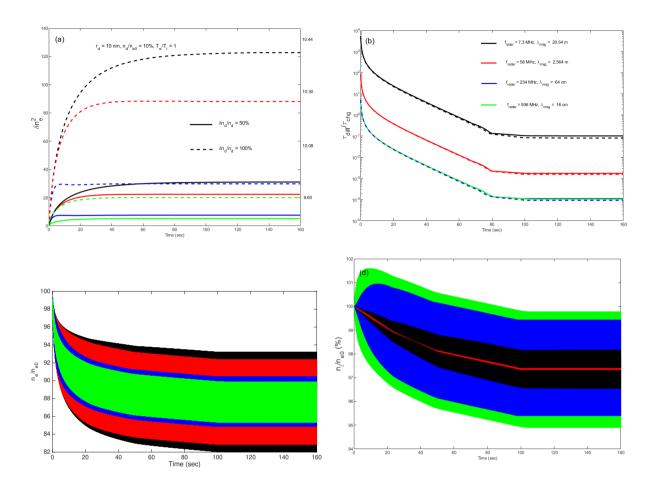
Figure 6. Similar to Figure 4 for $r_d = 10$ nm, $n_d/n_{e0} = 10\%$, and $T_e/T_i = 1$.

amplitude of electron density fluctuation and the associated radar echoes at different wavelengths. Another important parameter that was investigated is the initial amplitude of dust density irregularities produced through neutral air turbulence ($\delta n_d/n_d$). In the case of larger dust particles of the size of 10 nm, the steady state condition is satisfied in much shorter time in comparison to 3 nm dust particles. In this case the stable fluctuation amplitude is achieved within 80 sec from the equilibrium condition (quasi-neutral plasma in the absent of dust particles). This parameter manifests itself in the steady state amplitude of electron density fluctuations. An empirical relationship for the δn_e^2 with dust density for the same dust radius has been obtained using the numerical results. It has been shown that δn_e^2 increases by a factor of $(n_{d2}/n_{d1})^{(6/5)}$. Moreover, according to the numerical results the dust radius of 3 nm with density of 150 percent with respect to the background electron density ($n_e = 2 \times 10^9$ m^{-3}) can produce radar echoes of order 12.5 dB ($log10N_e$) for $f_r = 7.3$ MHz. This shows a close agreement with the experimental observations presented in Figure 1. More quantitative comparison of numerical results with the observations requires same
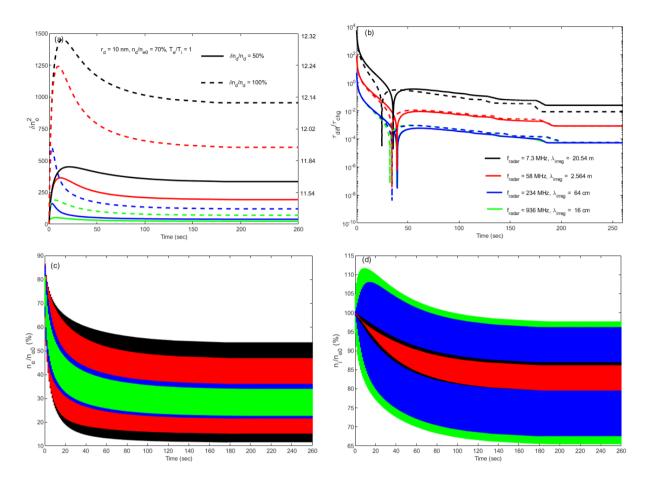
13

Figure 7. Similar to Figure 4 for $r_d = 10$ nm, $n_d/n_{e0} = 70\%$, and $T_e/T_i = 1$.

unit observations at all radar frequencies rather than normalized values (presented in this paper), which is the subject of future work.

265 One of the main features observed in the numerical simulations is that the electron density depletion is independent of the fluctuation wavelength and only varies with the background dust parameters. This effect validates the coherent scattering mechanism considered as the major source for plasma density irregularity generation. Therefore, it has been shown in this paper that the direct role of electron density depletion on corresponding radar echoes in various frequency bands is not possible, unlike the previous conclusion by Varney et al. (2011). In fact, the electron density fluctuation amplitude plays the major role in the

270 coherent scattering process. The numerical results associated with various background dusty plasma is considered in order to investigate the 8, 56, 224, and 930 MHz PMSEs.

Rapp et al. (2007) presented PMSE study at three radar frequencies for non-common regions and showed that the dust particles of 20 nm size are required to get the best agreement with the observations and theoretical model. Almost all recent

in-situ rocket observations of the PMSE source region in different months have shown ~~the~~ dust/ice particles at much smaller radius are responsible for the radar echoes. Moreover, AIM satellite observations have shown the similar concept. The present paper uses ~~the~~ state-of-the-art numerical model capable of simulating the PMSE source region including all important physical processes. The results presented in the paper have shown that even small dust particles are capable of producing ~~the~~ radar echoes at the same level as those observed in the experiment. Therefore, the proposed model and the novel observational results presented in this paper are an advancement to the field and previous works.

In-situ rocket and radar observations have proved that neutral air turbulence by itself has a minor effect on the creation of small scale plasma irregularities in the PMSE region. The rocket measurements have shown a sharp cut off of fluctuations of order a few tens of meters (~ 24 m) (Rapp and Lubken, 2003). The long lifetime of PMSE below the freezing altitude and even in the absence of neutral air turbulence have been attributed to frozen ~~structure~~ produced initially through turbulence advection and due to reduced diffusivity. The typical power spectrum of turbulence motion has two distinct parts. The first part represents a tracer with a wavenumber dependence of $k^{-5/3}$, which is known as the inertial subrange. The power spectrum continues with a second part where power spectrum is proportional to k^{-1}. Such spectral variation predicts a near zero power amplitude for a Bragg scale of ~ 5 m associated with $f_r \sim 56$ MHz due to dominant molecular diffusion. In general kinematic viscosity (diffusion of momentum) and turbulent energy dissipation rate (dissipation of turbulence energy to heat) are the two main parameters that affect the minimum scale of irregularities in the inertial subrange. Particles as large as 10 -15 nm around 85 km were proposed to justify the extended range of PMSE observations (Rapp and Lubken, 2003; La Hoz et al., 2006). The numerical simulations presented in this paper demonstrate the major role of dust density along with dust radius as the two main parameters that determine the general behavior of the turbulence power spectrum.

The general correlation of the shape of the PMSE at different frequencies obtained through the observations reveals the existence of ~~the~~ plasma density fluctuations and associated ~~structure~~ over the same altitude range. The high-resolution common-volume PMSE probed with 8 ~~MHz~~, 56 ~~MHz~~, 224 ~~MHz~~, and 930 MHz radars are observed for the first time. Figure 8a presents the actual amplitude of radar echoes over the HF PMSE altitude range (80.91 km to 91.4 km) on 26 July 2013 at 10:00 ~~UT~~, 11:00 ~~UT~~, 11:50 ~~UT~~, and 13:00 UT. Figure 8b also provides a summary of numerical results of radar echo associated with Figures 4-7 and corresponding to the variation of ~~the~~ radar echo strength with dust parameters. A close comparison between the two figures shows a good correlation in regards to strength consistency as the radar frequency increases from 8 ~~MHz~~ to 224 ~~MHz~~ and 930 MHz. Such averaging of radar echoes is essential to determine the effectiveness as well as durability of the original turbulence in the presence of dusty plasma to generate coherent echoes from 8 ~~MHz~~ to 930 MHz (although it is very rare to observe PMSE at 930 MHz). Larger dust particles of 10 nm as well as smaller particles (3 nm) are also taken into account to examine the hypothesis of the role of larger dust particles in the PMSE formation. The numerical results have shown that for similar dust parameters (r_d and n_d), the expected radar echoes (δn_e^2) are very close for 224 ~~MHz~~ and 930 MHz. It has been illustrated that the reduction of dust density fluctuation amplitude ($\delta n_d/n_d$) by a factor of 2 would reduce the expected radar echoes by 1 dB. The overall drop in the PMSE amplitude shows a similar drop as the $\delta n_d/n_d$ reduces from 1 to 0.5 for all dust parameters presented in Figures 4-7. Therefore, although according to the numerical results the estimated PMSE amplitude is similar for 224 ~~MHz~~ and 930 MHz, ~~the~~ $\delta n_d/n_d$ plays a critical role in the steady-state amplitude of irregularities
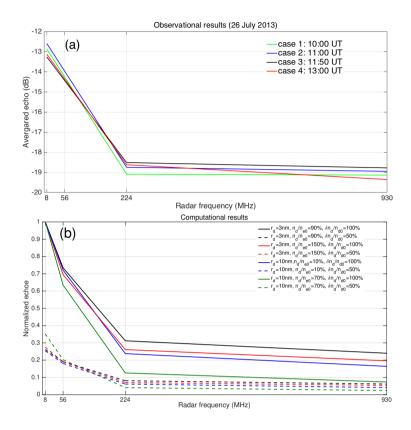
Figure 8. a) Averaged power echoes over the HF PMSE altitude range (in arbitrary ~~unit~~) ~~and associated with~~ 26 July 2013, in 4 cases at 10:00 ~~UT~~, 11:00 ~~UT~~, 11:50 ~~UT~~, 13:00 UT. b) Numerical results associated with Figures 4-7 and corresponding to the variation of the radar echo strength with dust parameters.

and associated PMSE. This validates the non-observation of UHF PMSE and can also be implemented to guide the previous
310   theories used to predict the neutral air turbulence spectrum in the presence of dust particles.

6   Conclusion

The first common volume observations of the PMSE source region with 4 radars including 8, 56, 224 and 930 MHz are presented in this paper. This is one of the main advantages of the present data in comparison with previous works (e.g. Rapp et al., 2007) that probed different regions of the PMSE (e.g. 130 km difference in PMSE location). Another main advantage
315   of the present work is including the HF PMSE observations at 8 MHz (corresponding to 20 m wavelength). This is critical to make a correct judgment on the applied theories such as neutral turbulence with high Schmidt number.

   To provide remote sensing information of dusty plasma within the probed region as well as a clear explanation of radar echo weakening with increasing ~~the~~ radar frequency, numerical simulation of the natural PMSE is provided. The numerical simulations were set up with an initial amplitude of dust density fluctuations of 50 or 100 percent with respect to the background

320 dust density. The values are selected based on recent observations and available theories. The physical processes including the competing charging and diffusion process to evolve during the simulation of the model. The charging on to the dust particles tends to increase the electron density fluctuation amplitude. The diffusion process tends to have the opposite impact. It has been shown that dusty plasma with $r_d = 3$ nm and $n_d = $ of 150 percent with respect to the background electron density ($n_e = 2 \times 10^9$ m^{-3}) can produce radar echoes with the same magnitude as the observations. While theoretical models fall short in predicting

325 the dusty plasma parameters associated with the observed PMSEs, a computational model is used in this paper to determine the background parameters as well as provide an explanation for the non-existence (strong weakening) of PMSE at 930 MHz.

The actual amplitude of radar echoes over the HF PMSE altitude range (80.91 km to 91.4 km) on 26 July 2013 at 10:00 UT, 11:00 UT, 11:50 UT, 13:00 UT are obtained. The numerical results of radar echo corresponding to the variation of the radar echo strength with dust parameters are calculated. A close comparison shows a good correlation in regards to radio echo

330 strength as the radar frequency increases from 8 MHz to 224 MHz and 930 MHz. The radar echo averaging is essential to determine the effectiveness as well as durability of the original turbulence in the presence of dusty plasma to generate coherent echoes from 8 MHz to 930 MHz (although it is very rare to observe PMSE at 930 MHz). It has been shown that the reduction of dust density fluctuation amplitude ($\delta n_d/n_d$) by a factor of 2 would reduce the expected radar echoes by 1 dB. This implies a new mechanism for non-observation of the UHF PMSE and can also be implemented to guide the previous theories used

335 to predict the neutral air turbulence spectrum in the presence of dust particles. Moreover, the numerical results showed the possibility that small dust particles (3 nm) may explain the observed radar echoes. Since the simple analytical models fall short in providing an explanation for the observed radar echoes and required the presence of large dust particles (20 nm) to justify the PMSE turbulence at different radar frequencies.

References

Batchelor, G. K. (1959), Small-scale variation of convected quantities like temperature in turbulent fluid. Part 1: General discussion and the case ofsmall conductivity,J. Fluid Mech.,5, 113–133.

Birdsall, C. K., and A. B. Langdon (1991), Plasma Physics Via Computer Simulation, McGraw-Hill, New York.

Chen, C., and Scales, W. A. (2005), Electron temperature enhancement effects on plasma irregularities associated with charged dust in the Earth's mesosphere, J. Geophys. Res., 110, A12313, doi:10.1029/2005JA011341.

Cho, J. Y. N., and Kelley, M. C. (1992), Enhancement of Thomson scatter by charged aerosols in the polar mesosphere: Measurements with a 1.29-GHz radar. Geophysical Research Letters, 19, 1097–1100.

Cho, J. Y. N. and Kelley, M. C. (1993), Polar mesospheric summer radar echoes: Observations and current theories, Rev. Geophys., 31, 243–265.

Cho, J. Y. N. and Rottger, J. (1997), An updated review of polar mesospheric summer echoes: Observation, theory, and their relationship to noctilucent clouds and subvisible aerosols, J. Geophys. Res., 102, 2001–2020.

Christon, S. P., Hamilton, D. C., Plane, J. M. C., Mitchell, D. G., Grebowsky, J. M., Spjeldvik, W. N., and Nylund, S. R. (2017), Discovery of suprathermal ionospheric origin Fe+ in and near Earth's magnetosphere. Journal of Geophysical Research: Space Physics, 122, 11,175–11,200. https://doi.org/10.1002/2017JA024414

Ecklund, W. L., and Balsley, B. B. (1981), Long-term observations of the Arctic mesosphere with the MST radar at Poker Flat, Alaska. Journal of Geophysical Research, 86, 7775–7780.

Havnes, O, H Pinedo, C La Hoz, A Senior, TW Hartquist, MT Rietveld, and MJ Kosch (2015), A comparison of overshoot modeling with observations of polar mesospheric summer echoes at radar frequencies of 56 and 224 MHz, Ann. Geophys., 33(6), 737–747

Hill, R. J. (1978), Non neutral and quasi-neutral diffusion of weakly ionized multi constituent plasma, J. Geophys. Res.,83, 989–998.

Hill, R. J., Gibson-Wilde, D. E., Werne, J. A., and Fritts, D. C. (1999), Turbulence-induced fluctuations in ionization and application to PMSE, Earth Plan. Space, 51, 499–513.

La Hoz, C., O. Havnes, L. I. Næsheim, and D. L. Hysell (2006), Observations and theories of Polar Mesospheric SummerEchoes at a Bragg wavelength of 16 cm,J. Geophys. Res.,111, D04203, doi:10.1029/2005JD006044.

Lie-Svenson, O., Blix, T. A., and Hoppe, U. P. (2003), Modeling the plasma response to small-scale aerosol particle perturbations in the mesopause region, J. Geophys. Res., 108, 8442, doi:10.1029/2002JD002753.

Lubken, F., Hillert, W., Lehmacher, G., and von Zahn, U. (1993), Experiments revealing small impact of turbulence on the energy budget of the mesosphere and lower thermosphere, J. Geophys. Res., 98, 20 369–20 384.

Lubken, F.-J., Rapp, M., Blix, T., and Thrane, E. (1998), Microphysical and turbulent measurements of the Schmidt number in the vicinity of polar mesosphere summer echoes, Geophys. Res. Lett., 25, 893–896.

Lubken, F.-J., Rapp, M., and Hoffmann, P. (2002), Neutral air turbulence and temperatures in the vicinity of polar mesosphere summer echoes, J. Geophys. Res., 107 (D15), doi:10.1029/2001JD000915.

Mahmoudian, A., Scales, W. A., Kosch, M. J., Senior, A., and Rietveld, M. (2011), Dusty space plasma diagnosis using temporal behavior of polar mesospheric summer echoes during active modification. Annales Geophysicae, 29, 2169–2174. https://doi.org/10.5194/angeo-29-2169-2011.

Mahmoudian, A., Mohebalhojeh, A. R., Farahani, M. M., Scales, W. A., and Kosch, M. (2017a), Remote sensing of mesospheric dust layers using active modulation of PMWE by high-power radio waves. Journal of Geophysical Research: Space Physics, 122, 843–856. https://doi.org/10.1002/2016JA023388.

Mahmoudian, A., Mohebalhojeh, A. R., Farahani, M. M., Scales (2017b), On the source of plasma density and electric field perturbations in PMSE and PMWE regions, Journal of the Earth and Space Physics, Vol. 42, No. 4, PP. 63-71

Mahmoudian, A., Senior, A., Scales, W. A., Kosch, M. J., and Rietveld, M. T. (2018), Dusty space plasma diagnosis using the behavior of polar mesospheric summer echoes during electron precipitation events. Journal of Geophysical Research: Space Physics, 123, 7697–7709. https://doi.org/10.1029/2018JA025395

Næsheim, L. I., O. Havnes, and C. La Hoz (2008), A comparison of polar mesosphere summer echo at VHF (224 MHz) and UHF (930 MHz) and the effects of artificial electron heating, J. Geophys. Res., 113, D08205, doi:10.1029/2007JD009245.

Pinedo, H., C. La Hoz, O. Havnes, and M. Rietveld (2014), Electron-ion temperature ratio estimations in the summer polar mesosphere when subject to HF radio wave heating, J. Atmos. Sol. Terr. Phys., 118, 106–112, doi:10.1016/j.jastp.2013.12.016.

Rapp, M., and Lubken, F. J. (2004), Polar mesosphere summer echoes (PMSE): Review of observations and current understanding. Atmospheric Chemistry and Physics, 4, 2601–2633.

Robertson, S., Horanyi, M., Knappmiller, S., Sternovsky, Z., Holzworth, R., Shimogawa, M., Friedrich, M., Torkar, K., Gumbel, J., Megner, L., Baumgarten, G., Latteck, R., Rapp, M., Hoppe, U.-P., and Hervig, M. E.: Mass analysis of charged aerosol particles in NLC and PMSE during the ECOMA/MASS campaign, Ann. Geophys., 27, 1213–1232, doi:10.5194/angeo-27-1213-2009, 2009

Scales, W. (2004), Electron temperature effects on small-scale plasma irregularities associated with charged dust in the Earths mesosphere. IEEE Transactions on Plasma Science, 32, 724.

Scales, W. A., and Mahmoudian, A. (2016), Charged dust phenomena in the near Earth space environment. Reports on Progress in Physics, 79(10), 106802. https://doi.org/10.1088/0034-4885/79/10/106802

Senior, A., Mahmoudian, A., Pinedo, H., La Hoz, C., Rietveld, M. T., Scales, W. A., and Kosch, M. J. (2014), First modulation of high-frequency polar mesospheric summer echoes by radio heating of the ionosphere. Geophysical Research Letters, 41, 5347–5353. https://doi.org/10.1002/2014GL060703

Varney, R. H., Kelley, M. C., Nicolls, M. J., Heinselman, C. J., and Collins, R. L. (2011), The electron density dependence of polar mesospheric summer echoes, J. Atmos. Sol.-Terr. Phys., 73, 2153–2165, doi:10.1016/j.jastp.2010.07.020, 2011.